THE JOURNAL OF PHYSICAL CHEMISTRY B

Article

pubs.acs.org/JPCB

Capacitance Spectroscopy: A Versatile Approach To Resolving the Redox Density of States and Kinetics in Redox-Active Self-Assembled Monolayers

Paulo R. Bueno,*[,†] Giulia Mizzon,[‡] and Jason J. Davis*[,‡]

[†]Instituto de Química, Universidade Estadual Paulista, CP 355, 14800-900, Araraquara, São Paulo, Brazil

[‡]Department of Chemistry, University of Oxford, South Parks Road, Oxford OX1 3QZ, U.K.

Supporting Information

ABSTRACT: Redox active self-assembled monolayers inherently possess both electrochemically addressable and polarizable components. The latter will contribute, with additional parasitic terms, to the *iR* drop effects within any form of electronic analysis, potentially distorting results. A capacitive analysis of such interfaces (Electroactive Monolayer Capacitance Spectroscopy), presented here, enables a clean mapping of both the thermodynamic and kinetic faradaic characteristics in a single experimental run, with parasitic nonfaradaic contributions (polarization and resistance terms) both spectrally resolved and cleanly removed. The methodology enables a rapid and undistorted quantification of accessible redox site density of states (reported directly by redox capacitance), molecular surface coverage, electron transfer kinetics, and reorganization energies with comparatively little experimental effort. Exemplified here with electroactive copper protein and ferrocene films the approach is equally applicable to any redox active interface.

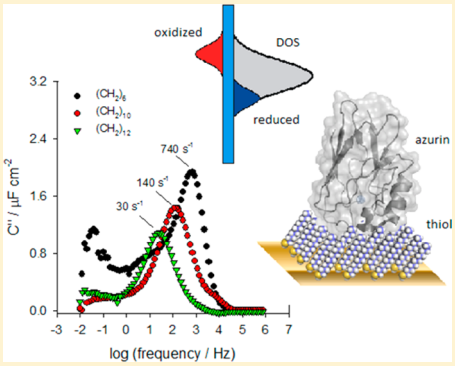

1. INTRODUCTION

The on-electrode assembly and analysis of redox active films provides a powerful means of analyzing, and indeed tuning, the thermodynamics and kinetics associated with molecular electron transfer, and an enormous amount of work has now been published with, for example, surface assembled transition metal complexes, organic molecules, and molecular wires.[1] An extrapolation of this approach to biomolecular films facilitates not only a decoding of their natural electron transfer properties (many of which are essential to sustaining life) but also, in a number of specific cases, derived biosensing configurations of real clinical or environmental value. The robust electrochemical addressing of these systems, greatly aided through considerations of surface charges, hydrophobic patches, and general issues of conformational stability, has been achieved at a variety of modified electrode interfaces.[2] Though the buried nature of many redox sites makes communication commonly difficult or sluggish, even after such optimization, analyses have become increasingly sophisticated during the past decade and, in some cases, molecularly resolved.[3] The premodification of electrodes with self-assembled monolayers (SAMs) for such work is integral in not only buffering potentially denaturing protein fold-electrode interactions but also in facilitating a control of molecular orientation and electron transfer kinetics.[4]

Redox-active SAMs provide an excellent platform for investigating electron transfer kinetics since the spatial and electronic coupling of these sites to underlying electrodes can be tightly controlled. Such layers have been extensively analyzed by *dc* cyclic voltammetry,[5] potential step chronoamperometry,[6] impedance/ac spectroscopy,[4a,5a,7] and laser induced temperature jump methods.[8] These approaches, each typified by specific strengths and limitations, can be divided into those which are frequency-resolved and those which are time-resolved (or transient). The latter are well understood and commonly applied to kinetic determinations despite the fact that the effects of SAM polarization and *iR* drop inherently contribute in an unknown (largely) and potentially grossly distorting manner. Frequency-resolved techniques such as impedance spectroscopy and alternating current voltammetry (ACV) operate in a manner which enables a clean resolution of contributing processes according to their time scales. ACV is similar to Cyclic Voltammetry (CV) in that it is a potential sweep method[9] but with an additional, frequency tuned, small perturbation of the AC oscillatory wave superimposed on the potential waveform. The resulting alternating current is recorded, and the electrochemical response appears as a single peak. Using this approach, for example, Creager and Wooster[4a] have developed a method of determining SAM electron transfer rates by collecting a series of AC voltammograms for a range of AC frequencies, where the ratio of the peak current (i_p) to the background current (i_b) is determined for each frequency. The values of i_p/i_b are plotted versus the logarithmic form of AC

Received: April 17, 2012
Revised: June 1, 2012
Published: June 11, 2012

   dx.doi.org/10.1021/jp303700f | *J. Phys. Chem. B* 2012, 116, 8822–8829

frequency, and these plots fitted to a Randles-like circuit model[4a] from which double-layer capacitance and charge transfer resistance are resolved and used in the determination of electron transfer rates (k). A number of reports have, subsequently, used this methodology,[10] though it suffers from the fact that the first input variables (double-layer capacitance, charge transfer resistance, electrode surface area, and solution resistance) must be determined previously from CV or Electrochemical Impedance Spectroscopy (EIS).

One advantage of ACV is that its inherent sensitivity enables films of very low surface coverage to be analyzed.[4a,10b,c] The methodology suffers, however, from frequency dependent fitting inaccuracies[11] and provides no information on reorganization energy or SAM polarization effects.

The large amplitude FT AC method introduced by Bond et al.[4b] is powerful in enabling the experimental resolution of electron transfer kinetics and thermodynamics. Its application is, however, neither steady-state nor achievable through standard hardware configurations. Its resolution of polarization terms has not been demonstrated.[4b]

EIS is a frequency-resolved and steady-state technique, because the voltage perturbations are inherently small and applied after the interface has equilibrated. Within these experiments the frequency response of a system is sampled by measuring the impedance function, $Z^*(\omega)$, a complex function. This is done by applying a small (1−10 mV) AC amplitude signal over a range of frequencies (typically MHz to mHz) at specified potentials. In tuning the frequency one controls the relative contribution of all contributing resistance and capacitance terms to the overall impedance. In doing this over a wide range of frequencies, the individual elements of the Randles-like circuit model can be separately resolved. It is important to observe that the Randles circuit is one of the simplest models for electron transfer for a redox species attached to a monolayer, and its applications must be carefully considered during EIS analysis (see below). It remains, nonetheless, dominantly applied within EIS studies of redox-active SAMs.[9,12]

As is the case with any complex function, impedance $Z^*(\omega)$ can be represented within either a Bode plot or a Nyquist plot. In Bode plots, the log of the magnitude of the impedance ($|Z|$), phase (φ) or the real (Z') and imaginary (Z'') components are plotted separately versus the logarithmic frequency. In a Nyquist, or complex-plane impedance diagram, the ordinate is the imaginary component of the impedance (Z'') and the abscissa the real component (Z'). The advantage of using an EIS approach, then, is that many parameters, such as electrolyte resistance, double-layer capacitance, charge transfer resistance, electrode surface area, and surface coverage, can be measured in one experiment. Problems may, however, arise due to the nonideal behavior of resistances (charge transfer) and capacitances (double-layer) of the system under study or by the limitations imposed through the use of an overly simplistic Randles-like circuit (that, for example, ignores SAM polarization contributions − see below), effects which can significantly distort derived parameter values in subsequent modeling.[1]

In aiming to develop a versatile and self-consistent approach to studying the electron transfer kinetics and redox density of states of electrode-confined films, the main purpose of the present work is not to reveal new facts about the specific redox systems utilized but to introduce and examine the utility of a purely capacitative frequency-resolved and steady-state methodology that is capable of mapping out the redox characteristics of molecular films generally. It will be shown that the proposed approach not only accurately maps these characteristics in a single step but, additionally, does so while resolving and correcting for contributions from nonfaradaic polarization and uncompensated resistance, without parameter input from other methodologies (i.e., the method is self-consistent). The approach also avoids the need to fit acquired data to an assumed Randles-like circuit.[1] Significantly the method also maps out the polarizable characteristics of the nonelectroactive components of the film, the density of accessible redox states present, and the electrochemical reorganization energy (film characteristics not as readily or cleanly derived from any single existing alternative method) from data typically acquired within minutes. Nearly all this information is acquired from measurements at only two fixed electrode potentials (one inside the redox potential window and one outside).

To exemplify the method, results obtained with films of azurin, a well-studied, conformationally stable, blue copper protein that can be coupled to metallic gold electrodes through alkyl thiol SAMs with orientational control (Figure 1), and ferrocene[6,13] are presented.

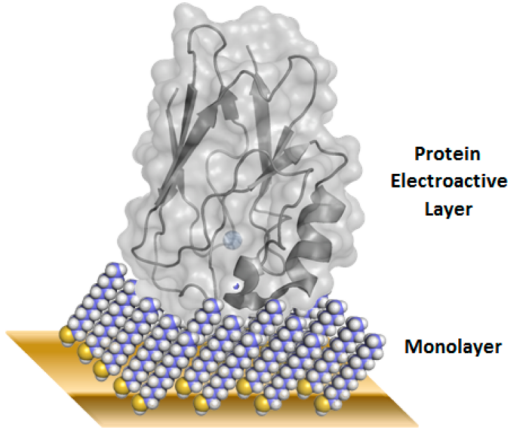

Figure 1. Schematic representation of the protein azurin coupled to an underlying metallic gold electrode through an alkyl thiol SAM. Such films were used herein as model bioelectronic layers, where electronic coupling and electron transfer rates could be tuned in a well-understood manner, and analyzed by Electroactive Monolayer Capacitance Spectroscopy (EMCS).

2. BACKGROUND THEORY

2.1. Complex Capacitance Spectroscopy. As mentioned in the experimental procedures (see the Supporting Information, SI.1), the complex $Z^*(\omega)$ (impedance) function is converted into $C^*(\omega)$ (capacitance) by $C^*(\omega) = 1/j\omega Z^*(\omega)$ (SI.2 for details). Practically, this involves taking the data resolved in a standard impedance analysis ($Z^*(\omega)$), sampled across a range of frequencies at any steady-state potential, and converting it phasorially into complex capacitance ($C^*(\omega)$) with its real and imaginary components.

Within this sampled complex capacitance both faradaic and nonfaradaic processes contribute, the latter being considered "parasitic" (see below). The interfacial capacitance of a monolayer dielectric modified electrode is defined, in the first instance, by two series capacitances, that of the monolayer (C_m) and that of the double-layer (C_{dl}). Additionally, the monolayer has an associated ionic polarization term composed of R_t and C_t

dx.doi.org/10.1021/jp303700f | J. Phys. Chem. B 2012, 116, 8822−8829

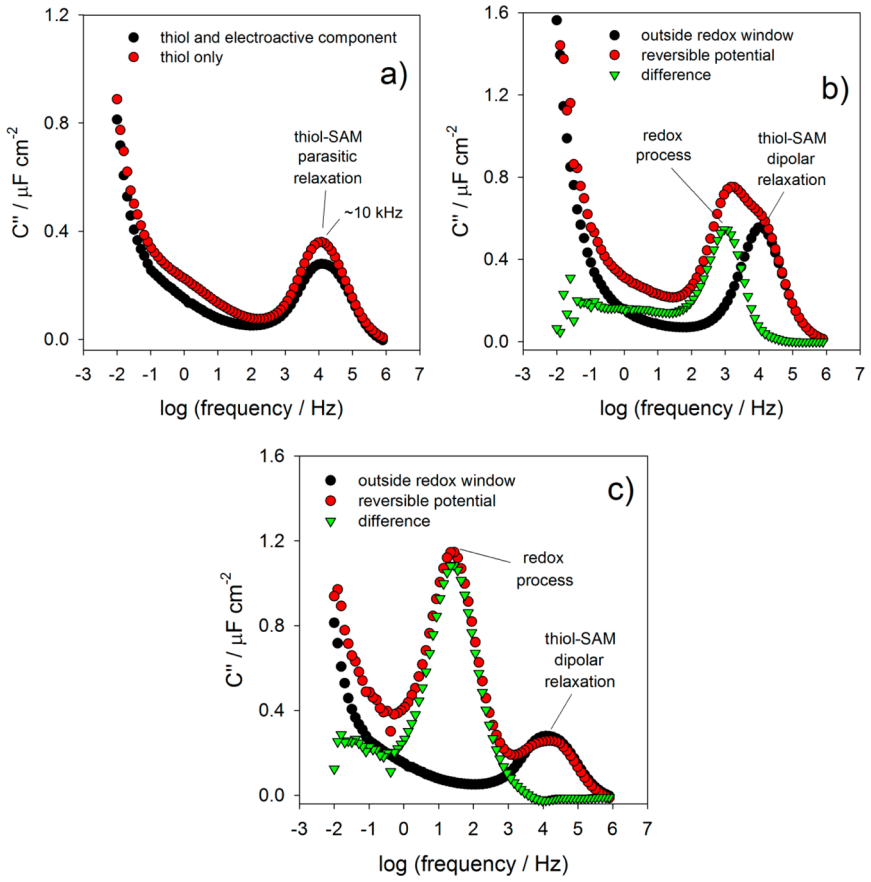

Figure 2. a) The imaginary part of complex capacitance of a nonredox active film (inherently so or at surface potentials outside of the redox window; here an electroactive azurin-on-hexanethiol film at −200 mV vs SCE) resolves the parasitic charging and resistance contributions that can, then, serve as a baseline that can be subtracted from subsequent analyses. b) With the working electrode potential moved into a region of optimum faradaic activity (here 90 mV vs SCE, the redox site reversible potential) an additional redox process is resolved (red spectrum), and a subtraction of the parasitic characteristics isolated in a) generates the purely redox response (green spectrum). c) Same as b) but for an azurin-on-dodecanethiol film, where the kinetics are slow compared to the hexanethiol analogue. The frequency axis is reported here as the base ten exponents only for clarity.

contributions (in the Debye formalism, for more detail, please see ref 14). These nonfaradaic charging processes are not readily removed in standard *AC* or *DC* voltammetric methods (and accordingly contribute to what is termed "uncompensated resistance").[4b] Their combined response to a modulating field is describable by a relaxation time τ and is directly and separately resolved in the spectroscopic method described herein, specifically in the steady-state frequency domain regime of complex capacitance (see Figure 2*a*). As discussed below, films which are redox addressable possess an additional ability to store charge, a process that has its own specific associated time scale.

2.2. Visualization and Removal of SAM Polarization Contributions and *iR* Drop. Complex capacitance data are composed of faradaic and nonfaradaic (parasitic) film contributions only. It is important to reinforce here that the $C^*(\omega)$ function, as a complex function, can be represented in Bode or Nyquist forms in a manner analogous to $Z^*(\omega)$. The imaginary component (C'') plotted against sampling frequency specifically resolves the time scale of the respective "parasitic" contributions (which can accordingly be subtracted, for instance, see the green spectrum of Figure 2). This is possible through the acquirement of data collected with the electrode poised outside the redox window (i.e., when only nonfaradaic processes operate) or, alternatively, on analogous films without a redox component (Figure 2*a*). When the system is poised inside the redox window (here at 90 mV vs SCE) an additional redox process is activated i.e. both parasitic and redox contributions are evident (Figure 2 and see below). Note that the faradaic process is fast here due to the comparatively small spatial separation between the copper center and the underlying gold. It is, accordingly, convoluted with the inherently rapid "parasitic" polarization process. In using the response obtained outside the redox window as a background (where only the polarization response of the bridges are responding to the electrode perturbation), the "parasitic" polarization can be spectroscopically subtracted, as shown in Figure 2*c* (green spectrum). Significantly, then, in sampling the complex capacitance of a redox active film, it is possible to resolve the "parasitic" term (encompassing *iR* drop, C_m, R_t, C_t and C_{dl}) and separate it from the process of redox center charging. This methodology *does not* require that the parasitic and redox contributions operate on distinguishable time scales. The remaining peak response within C'' versus log frequency (Bode) plots is, thus, purely representative of redox charging within the monolayer.

2.3. Redox Capacitance and Marcus-Gerischer Theory. The redox center charging within redox active films (Figure 2) generates, then, a redox capacity, C_r,[15] defined by

$$C_r = -\frac{dQ}{dV} = Ae^2\Gamma\frac{df}{dE_F} \quad (1)$$

dx.doi.org/10.1021/jp303700f | J. Phys. Chem. B 2012, 116, 8822−8829

where $Q = Ane$, the total amount of charge injected at a given steady-state potential V (and thus Fermi energy E_F is $-edV = dE_F$), where e is the elementary charge, and A is the area of the electrode. f is an occupancy fraction (n/Γ, where n is the number density of redox states and Γ is the molar surface density), leading to a function peaking at the standard potential, at which ($f(n,E_0) = 1/2$), with a slope of 60 mV/decade at the cathodic/anodic sides. The ability of such films to discharge, and lose energy, through redox electron transfer is defined by a charge transfer resistance term, R_{ct} (quantifying the strength of electronic coupling of the redox sites to the underlying electrode). Note that, because data are acquired under steady-state conditions, faradaic activity is fully absorbed within these terms. The interpretation of R_{ct} from this theory will be discussed elsewhere.

C_r and R_{ct} terms are correlated by the frequency of the charge transfer process (f_r) in a manner that can be developed from the Marcus-Gerischer theory which takes into account the DOS structure of the electrode where the Fermi level lies within a broad energy band of allowed states. Within this scheme the redox capacitance directly reflects both the redox site Density of States, as schematically depicted in Figure 3, and the electrodes

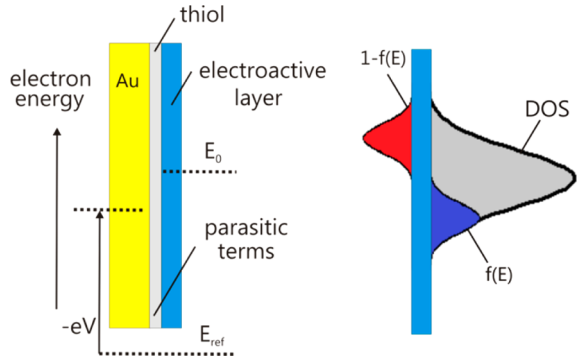

Figure 3. Schematic representation of a modified electrode interface composed of dielectric (C_m, R_t, and C_t) and redox-active regions. The former, together with the double layer (not shown) contributes to "parasitic" (resistive and capacitive) terms in any electrochemical analysis. We demonstrate herein that these contributions can be spectroscopically resolved and separated from those which are redox related in Electroactive Monolayer Capacitance Spectroscopy (EMCS) experiments. In analyzing the isolated "redox capacitance" as a function of surface potential, one can directly resolve the associated oxidized $[1 - f(E_0 - E_F)]$, reduced $f(E_0 - E_F)$, and total accessible redox Density of States (DOS) at any given potential. Data shown on the right have been extracted experimentally from an azurin film on decanethiol at the electrochemical half wave potential (where the reduced and oxidized states integrate equivalently).

ability to change it. It is important to note, then, that the redox capacitance is a dynamic term reflecting not only the occupancy of redox states across the electrode surface (describable by a Fermi-Dirac distribution function) but also their coupling to the electrode states (the rate of change of redox occupancy with electrode potential, $f(E)$)

$$f(E_0 - E_F) = \frac{1}{1 + \exp[(E_0 - E_F)/k_BT]} \tag{2}$$

The redox capacitance of the surface can, therefore, be expressed as

$$C_r = \frac{Ae^2\Gamma}{k_BT} f(1 - f) \tag{3}$$

Integrating this function over all energies, E, generates a capacitance that directly reflects film redox composition

$$C_{r,A} = e^2 \int_{-\infty}^{+\infty} D(E) \frac{df}{dE_F} dE \tag{4}$$

In now assuming that the Fermi-Dirac distribution is a step function, i.e. the zero-temperature approximation, $C_{r,A}$ (the redox capacitance per unit area) then takes the form

$$C_{r,A}(E_F) = e^2 D(E_F) \tag{5}$$

with $D(E_F)$, the electrode density of states at E_F, best modeled as a Gaussian function of site energies

$$D(E_0) = \frac{1}{\sigma\sqrt{2\pi}} \exp\left[-\frac{(E_0 - E_F)^2}{2\sigma^2}\right] \tag{6}$$

Here σ is the width of the distribution (the standard deviation), and E_0 is the center of the distribution (the electrochemical half wave potential). The former (σ) is related to λ, i.e. the reorganization energy, by $(2\lambda k_BT)^{1/2}$. A C_r determination as a function of electrode potential then (eqs 5 and 6) directly maps onto both the accessible redox DOS and the distribution of redox states as a function of potential.

Finally, it is important to observe that f denotes the redox occupancy, and $f(1 - f)$ is the probability density of finding an empty state (reduced or oxidized probability functions are equivalent and do not need to be distinguished).[9] Eq 3 quantifies the probability of finding an empty redox state of energy $E_0 - E_F$ on the electrode surface. It follows that the maximum of eq 3 occurs when $f = 1/2$ and $(1 - f) = 1/2$ leading to a $f(1 - f)$ probability density function having a maximum of 1/4.

3. RESULTS AND DISCUSSION

3.1. Resolving a Corrected Redox Response. Prior to capacitative analyses, the electrochemical reversible potential and redox window are initially defined, in the same experimental configuration, by a single cyclic voltammogram. This procedure is only necessary if one does not prior know the redox potential window of the studied system and serves only this purpose. After this, impedance measurements are conducted at only two steady-state potentials, i.e. the potential in which the current peak potential is maximum (the reversible potential where $f(1 - f)$ has a maximum of 1/4 and the redox activity is maximum) and in any other potential outside of the redox window, where only the monolayer "parasitic" contributions are observed (Figure 2*a*). The monolayer "parasitic" processes, as previously noted, operate on a fast (~10 kHz, Figure 2*a*) time scale independent of surface potential and can be readily subtracted from the measured contributions of redox activity. As previously discussed within Figure 2*b*, this subtraction is effective *even if these contributions do not operate on clearly separable time scales* (which may be the case if faradaic electron transfer is very fast, as shown in Figure 2*b*) by simply acquiring data at the reversible potential (where redox site occupation by electrons, $f = 1/2$) and at a potential outside of this (where the occupation function $f = 0$ or $f = 1$; in both cases the redox capacitance will be null according to eq 3, meaning that the obtained response will be exclusively due to "parasitic"

dx.doi.org/10.1021/jp303700f | J. Phys. Chem. B 2012, 116, 8822−8829

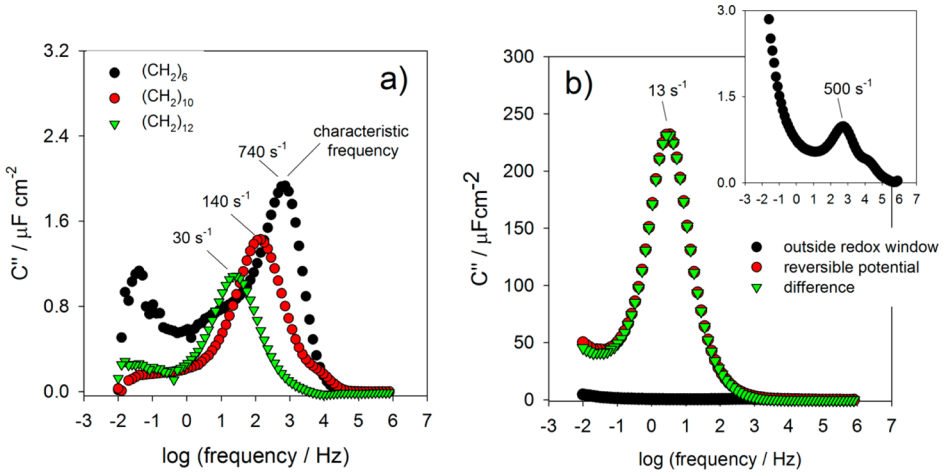

Figure 4. a) A comparative analysis of azurin films across three different supporting thiol layer thicknesses (hexanethiol, decanethiol, dodecanethiol) resolves clearly the characteristic frequencies of their associated redox capacitance charging. As with Figure 2, the frequency axis is labeled in base ten exponents for clarity. Any peak observed in such spectra is related to a characteristic charging process and directly reports its time scale. Contributions from redox sites are evident when the electrode potential is poised inside the redox window. Any charging process outside of this range is considered parasitic and can be subtracted (the data shown above are purely redox based). b) A redox capacitance analysis of an 11-ferrocene-undecanethiol film. The higher redox surface density and stronger electronic coupling in these redox films (compared to the metalloprotein films) is reflected in a redox contribution (red and green) that is some 2 orders of magnitude higher than the parasitic contributions. The peak frequency reports an electron transfer rate (13 $s^{-1} \pm 2$) is in good agreement with that determined by classical voltammetric methods (see SI.4). The inset reports the magnitude and time scale of the small parasitic contribution.

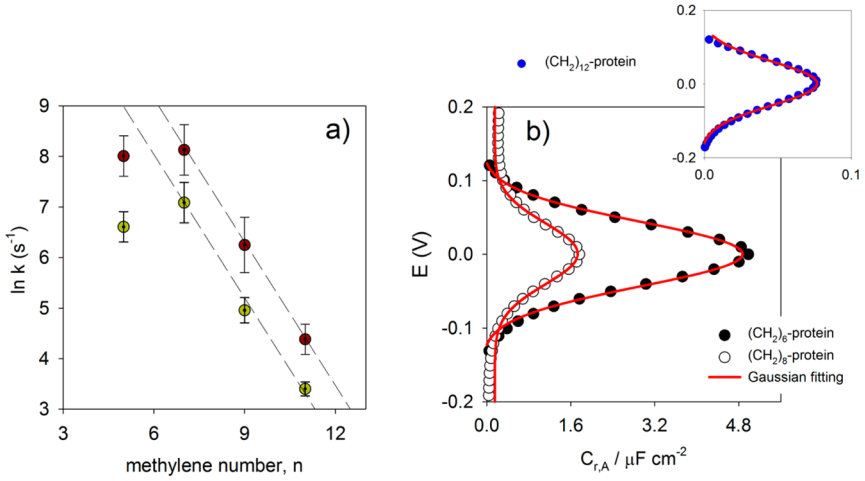

Figure 5. a) Capacitance derived electron transfer rates k for azurin molecular films plotted (dark yellow circles) as a function of the underlying SAM chain length. The gray lines represent guides to the eye for exponential decay functions with β of −0.90 and −0.93 per methylene unit in the nonadiabatic regime,[16c] respectively. Rates are shown comparatively from both CV analyses (dark red circles, more details can be found in the SI) and by EMCS (dark yellow circles). As expected, the rate of electron transfer reaches a plateau at short SAM lengths (points acquired for hexanethiol) where the electron transfer is now in the dynamically controlled limit.[16c,17] b) Redox capacitance versus potential obtained from EMCS analyses of an electroactive azurin layer on two different thiol SAM supports. Note that the accessible DOS, centered here at zero for convenience, depends on the sampling frequency (here 100 Hz) with a sensitivity that directly reflects the tunneling efficacy between the redox site and underlying electrode i.e. the electron transfer kinetics. The reduced value of $C_{r,A}$ observed at the same sampling frequency with a redox site further from the electrode is highlighted in the inset (azurin on a dodecanethiol support). The Gaussian fits to this data are consistently very good (chi-squared 0.99).

polarization processes). Since both monolayer dielectric and solution resistance contributions can be subtracted at this point, they make no contribution to the resolved redox response. For more details and exemplification of the subtraction of monolayer parasitic contributions see SI.8−10.

It is possible, then, to resolve and isolate both redox and nonredox contributions to electrode charging. Where redox sites are only weakly coupled to the underlying electrode, one expects and indeed observes that these processes operate on distinctly different time scales (Figure 2*c*).

3.2. Redox Kinetics from EMCS. Since the characteristic frequency of an isolated faradaic charging process equates to the electron transfer rate constant, one can seek to map this across different redox site − electrode coupling; Figure 4*a* shows the resultant spectra that resolve the time scales as ∼30 s^{-1}, ∼140 s^{-1}, and ∼740 s^{-1} for azurin on hexanethiol, decanethiol, and dodecanethiol supported films, respectively. These values correlate well with previous reports and concurrent cyclic voltammetric analyses on the same films (SI.2 and SI.4). The results of an equivalent analysis with a 11-ferrocenyl-undecanethiol film is shown Figure 4*b* (and SI.5).

dx.doi.org/10.1021/jp303700f | J. Phys. Chem. B 2012, 116, 8822−8829

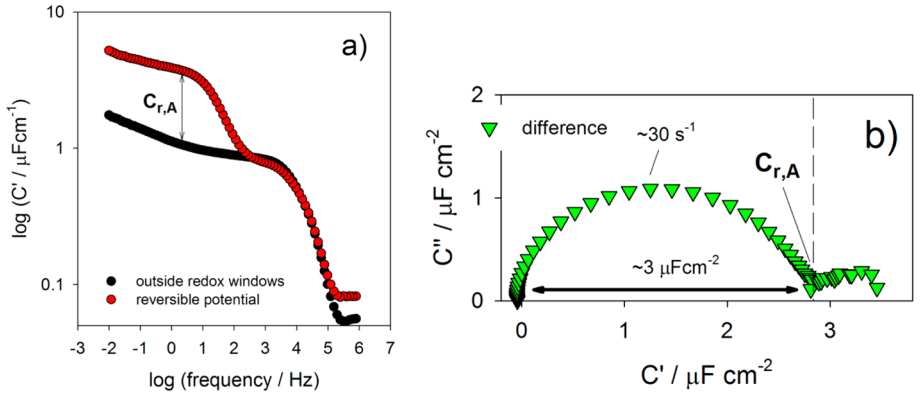

Figure 6. a) The real part of complex capacitance as a function of frequency for an azurin molecular film on dodecanethiol. With the electrode poised outside of the redox window only the high frequency parasitic terms contribute (black line). At, or close to, the half wave potential such analyses resolve the redox contribution at low frequency (red line). A subtraction of these contributions enables a quantification of $C_{r,A}$. Alternatively, b) shows a Nyquist capacitive plot of C'' versus C' where $C_{r,A}$ can be directly obtained from the diameter of the semicircle (plotted data are, again, the difference between that acquired at the half wave potential and outside of the redox window). Here $C_{r,A}$ is resolved by both methods to be 3 ± 0.3 μF·cm^{-2}.

These frequencies are expected, of course, to vary exponentially with tunneling distance, through the following: $k \propto Z \exp[-\beta(E_0)r]$. The β values derived herein for azurin sampled across a range of supporting alkenethiol films correlate very well with expectations (Figure 5*a*).

Interestingly, we observe small but systematic differences in the kinetic determinations by EMCS and traditional voltammetric methods for the same films (approximately four times higher for the latter). We believe this to be related to the contributory dielectric and ionic polarizable features not easily eliminated in the latter, standard, analyses.[4b] The dipolar relaxation contributions, specifically, cannot be eliminated by transient techniques such as CV nor can the contributions of *i*R drop be readily observed and removed (contributions which will distort determinations of k). The kinetic determinations we report herein are likely, then, to be more accurate.

3.3. Density of Redox States Determination. Once the timescale of the redox contribution to interfacial charging has been mapped by means of the C'' spectrum (reporting electron transfer kinetics), the redox capacitance per unit of area $C_{r,A}$ can be directly quantified via either of two means. In plotting the real part of complex capacitance (C') as a function of logarithmic frequency (Figure 6*a*) with the electrode poised inside then outside of the redox window, a subtraction directly reports $C_{r,A}$ (where the lines diverge at a frequency corresponding to the onset of redox electron transfer). Alternatively, $C_{r,A}$ can be obtained from the intercept of an equivalently generated Nyquist plot (Figure 6*b*).[14a]

The significance in quantifying $C_{r,A}$ is that its magnitude directly reflects the number of redox sites coupling to the underlying electrode (the redox site total DOS, as previously discussed; see eqs 4−6). The maximal value of $C_{r,A}$ (i.e. $C_{r,m}$) is obtained with the electrode poised at the reversible potential ($f(E_0) = 1/2$), and directly reports, through eq 7 (derived from eq 3 in considering $f = 1/2$ and $(1 - f) = 1/2$), the molecular surface coverage of the redox entity, Γ (derived here as 1.6 ± 0.2 pmol cm^{-2} for azurin on decanethiol, for example).

$$C_{r,m} = \frac{e^2\Gamma}{4k_BT} \tag{7}$$

3.4. Reorganization Energy determination. The Gaussian shapes of DOS and C_r derived and depicted in Figures 3 and 5*b* respectively contain not only information about the total accessible redox site DOS at any given frequency but also its constituent reduced and oxidized components. Once the total redox site DOS is obtained from eq 7, the oxidized and reduced subpopulations can be obtained through eq 3 at *any given potential* (see SI.7). In sampling C_r across a range of electrode potentials then, in a method similar but not equivalent to *AC* voltammetry (since the EMCS approach is alone in isolating a pure redox response free from *i*R drop contributions), a Gaussian function, representing the redox DOS, is generated as shown in Figure 5*b*. If the scan potential sweep is performed at frequencies that ensure the system is in redox equilibrium, a frequency that can be obtained from Bode analysis (Figure 4), the reorganization energy, λ, can be readily obtained from the (Marcus-Gerischer) relationship between this Gaussian DOS function.[9] λ is resolved here as ~0.30 eV ± 0.1 for azurin on all the thiols sampled, a value in very good agreement with that determined by traditional *interfacial* electrochemical methodologies.[16] The invariance of λ with thiol length is consistent with prior reports.[16c] A more detailed consideration of these DOS analyses within this EMCS framework is underway.

4. SUMMARY AND FINAL REMARKS

EMCS is proposed as a robust and experimentally simple steady-state technique from which a "clean" resolution of electron transfer kinetics, dielectric/charging contributions and addressable surface density, is obtained from just a single capacitance/impedance sampling inside the film redox window and one outside. The mapping of redox kinetics is robust for processes occurring across a broad range of frequencies (limited ultimately by the frequency window of EIS, typically 1 μs to 10 ks).

The advantage of this technique over ACV and impedance studies of redox films is that the method is facile and fully self-consistent, provides a detailed mapping of all current contributions, and requires no fitting to Randles-like equivalent circuits (with the assumptions that necessarily go with this). The method requires only that EIS measurements are performed at two potentials, from which $Z^*(\omega)$ and $C^*(\omega)$ complex functions are acquired with *i*R drop correction. In the complex capacitance domain, $C''(\omega)$ Bode capacitive plots

dx.doi.org/10.1021/jp303700f | J. Phys. Chem. B 2012, 116, 8822−8829

nicely resolve not only background polarization contributions but also the frequency of redox charging process, the latter directly equating to the (undistorted) faradaic charge transfer rate according to $k = f_r$. From equivalent $C'(\omega)$ Bode capacitive plots, C_r is directly obtained and enables both redox coverage and redox site DOS to be calculated − the latter facilitates a mapping of the redox composition of the film at any specific electrode surface potential. Furthermore, at suitably low sampling frequencies, such DOS plots enable the faradaic λ to be acquired.

In summary, we have presented herein a practically simple method that utilizes an entirely novel application of capacitative electrochemistry to map out the thermodynamic and kinetic characteristics of surface − confined electroactive films. The hardware required is minimal and standard for all the analysis conducted herein, the observations robust and in line with both expectations and prior analyses (though, notably without distortion), and the acquirement of electron transfer kinetics, molecular surface coverage, and reorganization energies with a clean separation of nonfaradaic contributions, in one sampling experiment, unprecedented. The methods, which are based on the isolation of redox contributions to interfacial capacitance, additionally and directly equate this capacitance with the sampling of redox activity across a range of energies (that is, report the redox film DOS) and are equally applicable to any redox active interface.

■ ASSOCIATED CONTENT

Ⓢ Supporting Information

Experimental procedures and methods and Figures S1−S12. This material is available free of charge via the Internet at http://pubs.acs.org.

■ AUTHOR INFORMATION

Corresponding Author

*P.R.B.: phone +55 16 3301 9642, fax +55 16 3322 2308, e-mail: prbueno@iq.unesp.br. J.J.D.: phone +44 1865 275914, e-mail jason.davis@chem.ox.ac.uk.

Notes

The authors declare no competing financial interest.

■ ACKNOWLEDGMENTS

This work was supported by the São Paulo state research funding agency (FAPESP) and São Paulo State University (UNESP) grants. The authors thank Professor Gerard Canters, Department of Physics, Leiden University, for a generous supply of azurin and Mr. Habibur Rahman for supplying raw ferrocene adlayer data.

■ REFERENCES

(1) Eckermann, A. L.; Feld, D. J.; Shaw, J. A.; Meade, T. J. Electrochemistry of redox-active self-assembled monolayers. *Coord. Chem. Rev.* **2010**, *254* (15−16), 1769−1802.

(2) (a) Armstrong, F. A.; Butt, J. N.; Sucheta, A. Voltammetric Studies of Redox-Active Centers in Metalloproteins Adsorbed on Electrodes. In *Methods in Enzymology*; Riordan, J. F., Vallee, B. L., Eds.; Academic Press: San Diego, 1993; Vol. *227*, pp 479−500. (b) Armstrong, F. A.; Hill, H. A. O.; Walton, N. J. Direct electrochemistry of redox proteins. *Acc. Chem. Res.* **1988**, *21* (11), 407−413. (c) Eddowes, M. J.; Hill, H. A. O. Novel method for investigation of electrochemistry of metalloproteins-cytochrome-C. *J. Chem. Soc., Chem. Commun.* **1977**, No. 21, 771−772. (d) Eddowes, M. J.; Hill, H. A. O.; Uosaki, K. Electrochemistry of cytochrome-C - Comparisons of the eletron-transfer at a surface-modified gold electrode with that to cytochrome-oxidase. *J. Am. Chem. Soc.* **1979**, *101* (23), 7113−7114.

(3) (a) Patil, A. V.; Davis, J. J. Molecular scale bioelectrochemistry. *Coord. Chem. Rev.* **2011**, *255* (17−18), 1970−1980. (b) Salverda, J. M.; Patil, A. V.; Mizzon, G.; Kuznetsova, S.; Zauner, G.; Akkilic, N.; Canters, G. W.; Davis, J. J.; Heering, H. A.; Aartsma, T. J. Fluorescent Cyclic Voltammetry of Immobilized Azurin: Direct Observation of Thermodynamic and Kinetic Heterogeneity. *Angew. Chem., Int. Ed.* **2010**, *49* (33), 5776−5779.

(4) (a) Creager, S. E.; Wooster, T. T. A new way of using ac voltammetry to study redox kinetics in electroactive monolayers. *Anal. Chem.* **1998**, *70* (20), 4257−4263. (b) Fleming, B. D.; Zhang, J.; Elton, D.; Bond, A. B. Detailed Analysis of the Electron-Transfer Properties of Azurin Adsorbed on Graphite Electrodes Using dc and Large-Amplitude Fourier Transformed ac Voltammetry. *Anal. Chem.* **2007**, *79*, 6515−6526. (c) Gaigalas, A. K.; Niaura, G. Measurement of electron transfer rates between adsorbed azurin and a gold electrode modified with a hexanethiol layer. *J. Colloid Interface Sci.* **1997**, *193* (1), 60−70.

(5) (a) Laviron, E. AC polarography and faradaic impedance of strongly adsorved electroactive species. 3. Theoretical complex-plane analysis for a surface redox reaction. *J. Electroanal. Chem.* **1979**, *105* (1), 35−42. (b) Laviron, E. General expression of the linear potential sweep voltammogram in the case of diffusionless electrochemical systems. *J. Electroanal. Chem.* **1979**, *101* (1), 19−28. (c) Weber, K.; Creager, S. E. Voltammetry of redox-active groups irreversibly adsorbed onto electrodes - Treatment using the Marcus relation between reate and overpotential. *Anal. Chem.* **1994**, *66* (19), 3164−3172.

(6) Chidsey, C. E. D. Free-energy and temperature-dependence of electron-transfer at the metal-electrolyte interface. *Science* **1991**, *251* (4996), 919−922.

(7) Nahir, T. M.; Bowden, E. F. The distribution of standard rate constants for electron transfer between thiol-modified gold electrodes and adsorbed cytochrome c. *J. Electroanal. Chem.* **1996**, *410* (1), 9−13.

(8) (a) Smalley, J. F.; Geng, L.; Chen, A.; Feldberg, S. W.; Lewis, N. S.; Cali, G. An indirect laser-induced temperature jump study of the influence of redox couple adsorption on heterogeneous electron transfer kinetics. *J. Electroanal. Chem.* **2003**, *549*, 13−24. (b) Smalley, J. F.; Geng, L.; Feldberg, S. W.; Rogers, L. C.; Leddy, J. Evidence for adsorption of Fe(CN)63-/4- on gold using the indirect laser-induced temperature-jump method. *J. Electroanal. Chem.* **1993**, *356* (1−2), 181−200.

(9) Bard, A. J.; Faulkner, L. R. *Electrochemical Methods Fundamentals and applications*, 2nd ed.; John Wiley & Sons: 2000; p 850.

(10) (a) Arikuma, Y.; Takeda, K.; Morita, T.; Ohmae, M.; Kimura, S. Linker Effects on Monolayer Formation and Long-Range Electron Transfer in Helical Peptide Monolayers. *J. Phys. Chem. B* **2009**, *113* (18), 6256−6266. (b) Okamoto, S.; Morita, T.; Kimura, S. Electron Transfer through a Self-Assembled Monolayer of a Double-Helix Peptide with Linking the Terminals by Ferrocene. *Langmuir* **2009**, *25* (5), 3297−3304. (c) Takeda, K.; Morita, T.; Kimura, S. Effects of monolayer structures on long-range electron transfer in helical peptide monolayer. *J. Phys. Chem. B* **2008**, *112* (40), 12840−12850.

(11) Li, J. H.; Schuler, K.; Creager, S. E. A generalized equivalent-circuit model for electroactive monolayers exhibiting a fixed redox potential and a distribution of electron-transfer rate constants - I. Square distributions. *J. Electrochem. Soc.* **2000**, *147* (12), 4584−4588.

(12) Bard, A. L.; Rubinstein, I. *Electrochemistry of Organized Monolayers of Thiols and Related Molecules on Electrodes*; Marcel Dekker, Inc.: New York, 1996.

(13) Chidsey, C. E. D.; Loiacono, D. N. Chemical Functionality in Self-Assembled Monolayers - Structural and Electrochemical Properties. *Langmuir* **1990**, *6* (3), 682−691.

(14) (a) Böttcher, C. J. F.; Bordewijk, P. *Theory of electric polarization. Dielectric in time-dependent fields*; Elsevier: Amsterdam, 1992; Vol. *II*. (b) Jonscher, A. K. The "universal" dielectric response. *Nature* **1977**, *267*, 673−679. (c) Jonscher, A. K. *Universal Relaxation Law*; Chelsea

Dielectric Press: London, 1996. (d) Goes, M. S.; Habibur, R.; Ryall, J.; Davis, J. J.; Bueno, P. R. A dielectric model of self-assembled monolayer interfaces by capacitance spectroscopy. *Langmuir* **2012**, DOI: http://dx.doi.org/10.1021/la301281y.

(15) (a) Bisquert, J. Physical electrochemistry of nanostructured devices. *Phys. Chem. Chem. Phys.* **2008**, *10* (1), 49−72. (b) Bisquert, J.; Fabregat-Santiago, F.; Mora-Sero, I.; Garcia-Belmonte, G.; Barea, E. M.; Palomares, E. A review of recent results on electrochemical determination of the density of electronic states of nanostructured metal-oxide semiconductors and organic hole conductors. *Inorg. Chim. Acta* **2008**, *361* (3), 684−698. (c) Chidsey, C. E. D.; Murry, R. W. Redox Capacity and Direct Current Electron Conductivity in Electroactive Materials. *J. Phys. Chem.* **1986**, *90*, 1479−1484.

(16) (a) Chi, Q. J.; Zhang, J. D.; Andersen, J. E. T.; Ulstrup, J. Ordered assembly and controlled electron transfer of the blue copper protein azurin at gold (111) single-crystal substrates. *J. Phys. Chem. B* **2001**, *105* (20), 4669−4679. (b) Guo, Y.; Zhao, J.; Yin, X.; Gao, X.; Tian, Y. Electrochemistry Investigation on Protein Protection by Alkanethiol Self-Assembled Monolayers against Urea Impact. *J. Phys. Chem. C* **2008**, *112*, 6013−6021. (c) Khoshtariya, D. E.; Dolidze, T. D.; Shushanyan, M.; Davis, K. L.; Waldeck, D. H.; van Eldik, R. Fundamental signatures of short- and long-range electron transfer for the blue copper protein azurin at Au/SAM junctions. *Proc. Natl. Acad. Sci. U. S. A.* **2010**, *107*, 2757−2762.

(17) Yokoyama, K.; Leigh, B. S.; Sheng, Y.; Niki, K.; Nakamura, N.; Ohno, H.; Winkler, J. R.; Gray, H. B.; Richards, J. H. Electron tunneling through Pseudomonas aeruginosa azurins on SAM gold electrodes. *Inorg. Chim. Acta* **2008**, *361* (4), 1095−1099.